Title

Autophagy-dependent production of secreted factors facilitates oncogenic RAS-driven invasion.

Journal

Cancer Discovery, 4(4)

Authors

Lock, Rebecca
Kenific, Candia
Leidal, Andrew
et al.

Publication Date

2014-04-01

DOI

10.1158/2159-8290.CD-13-0841

Peer reviewed

Published in final edited form as:
Cancer Discov. 2014 April ; 4(4): 466–479. doi:10.1158/2159-8290.CD-13-0841.

Autophagy dependent production of secreted factors facilitates oncogenic RAS-driven invasion

Rebecca Lock, **Candia M. Kenific**, **Andrew M. Leidal**, **Eduardo Salas**, and **Jayanta Debnath**
Department of Pathology, Helen Diller Family Comprehensive Cancer Center and Biomedical Science Graduate Program, University of California, San Francisco, California 94143, USA

Abstract

The tumor promoting functions of autophagy are primarily attributed to its ability to promote cancer cell survival. However, emerging evidence suggests that autophagy plays other roles during tumorigenesis. Here, we uncover that autophagy promotes oncogenic RAS-driven invasion. In epithelial cells transformed with oncogenic RAS, depletion of autophagy-related genes suppresses invasion in three-dimensional culture, decreases cell motility, and reduces pulmonary metastases *in vivo*. Treatment with conditioned media from autophagy-competent cells rescues the invasive capacity of autophagy-deficient cells, indicating these cells fail to secrete factors required for RAS-driven invasion. Reduced autophagy diminishes the secretion of the pro-migratory cytokine IL6, which is necessary to restore invasion of autophagy-deficient cells. Moreover, autophagy-deficient cells exhibit reduced levels of MMP2 and WNT5A. These results support a previously unrecognized function for autophagy in promoting cancer cell invasion via the coordinate production of multiple secreted factors.

Keywords

Autophagy; RAS; Invasion; Three-dimensional culture; Secretion; Interleukin 6

INTRODUCTION

The RAS proteins are members of a family of small GTPases critical in mediating cellular responses following activation by upstream extracellular signals, such as growth factors. Oncogenic mutations in RAS, which result in constitutive activation, are found in approximately 30% of human cancers; they are highly prevalent in several carcinomas, including lung, pancreas, and colon (1, 2). Notably, oncogenic RAS drives diverse cellular programs-proliferation, cell survival, migration, invasion and alterations in differentiation-that support tumor initiation and progression. Such mutations present a formidable therapeutic obstacle, because patients harboring mutant KRAS are refractory to most available systemic therapies and exhibit extremely poor survival (2). Hence, identifying new processes to target cancer cells with hyperactive RAS remains a question of immense clinical significance. One such pathway may be macroautophagy (autophagy), a tightly controlled lysosomal degradation process that promotes cell survival during nutrient

Correspondence to: Jayanta Debnath, M.D., University of California San Francisco, 513 Parnassus Ave, HSW 450B (Box 0502), San Francisco, California 94143, Phone: 415-476-1780, FAX: 415-514-0878, Jayanta.Debnath@ucsf.edu.

Conflicts of interest: The authors have no conflicts of interest to disclose.

CONTRIBUTIONS

RL, CMK, AML and JD designed the experiments. RL, CMK, AML, ES and JD carried out the experiments as well as analyzed and interpreted results. JD supervised the overall study. RL and JD wrote the paper with comments from the other authors.

starvation and stress. Recent evidence indicates that basal autophagy levels are enhanced upon oncogenic RAS activation and support RAS-driven transformation and tumorigenesis (3-7).

The tumor promoting functions of autophagy are largely ascribed to its importance as a survival pathway in response to diverse environmental stresses (8, 9). For example, enhanced autophagy is observed in poorly perfused, hypoxic tumor regions and loss of autophagy is associated with increased necrosis (10). Autophagy also promotes tumor cell survival in response to various cytotoxic and targeted chemotherapies (11). Importantly, studies of oncogenic RAS transformation have revealed that the pro-tumor effects of autophagy are not limited to increased survival of cancer cells under duress; rather, autophagy contributes to the metabolic fitness of the entire tumor population (3-6). Because strong oncogenic insults, such as RAS activation, are marked by profound metabolic alterations that drive both energy production and biosynthetic capacity in rapidly proliferating cells, it has been hypothesized that autophagy maintains key metabolic pathways in RAS-transformed cells. In support, a growing body of work has unveiled a requirement for autophagy in driving proliferation as well as sustaining multiple core metabolic functions in RAS-transformed cells (3-7). These results are not unique to oncogenic RAS activation, as deletion of *RB1CC1/FIP200*, a mediator of autophagosome initiation, inhibits polyoma middle T driven mammary cancer, due to reduced proliferation and glucose metabolism (12).

In addition to its effects on proliferation and metabolism, oncogenic RAS drives diverse aggressive cellular behaviors that support tumor progression and metastasis; importantly, RAS-transformed epithelial cells exhibit highly invasive behavior associated with an epithelial-to-mesenchymal transition (EMT) (13). Here, in epithelial cells transformed with oncogenic RAS, we demonstrate that autophagy facilitates extracellular matrix (ECM) invasion, tumor cell motility, and pulmonary metastasis in vivo. Using a three-dimensional (3D) culture system, we uncover that autophagy inhibition restricts RAS-driven cell invasion and restores several aspects of normal epithelial architecture, including the polarized deposition of basement membrane and cell-cell junctional integrity. Furthermore, autophagy is required for the production of multiple secreted factors in RAS transformed cells, including interleukin-6 (IL6), matrix metalloproteinase 2 (MMP2), and WNT5A, which altogether facilitate cancer cell invasion.

RESULTS

Autophagy promotes invasion driven by oncogenic RAS in 3D culture

To elucidate how autophagy impacts the cellular behavior of RAS-transformed epithelial cells, we utilized the MCF10A 3D epithelial culture system to interrogate how autophagy affects the growth and morphogenesis of cells expressing oncogenic RAS (14). We generated stable pools of MCF10A human mammary epithelial cells expressing a control vector (BABE) or an oncogenic form of HRAS ($HRAS^{V12}$) that enhances basal autophagy and elicits robust anchorage independent transformation (3). When cultured on laminin-rich ECM, control MCF10A cells formed hollow, spherical acini (Fig. S1A) (15). In contrast, $HRAS^{V12}$ transformed cells produced grossly aberrant structures notable for extensive protrusions that invaded the surrounding extracellular matrix. Individual $HRAS^{V12}$ structures formed these invasive protrusions as early as 3-5 days, ultimately producing disorganized networks of cells intermingled with large cell clusters after 8 days in 3D culture (Fig. 1A and B, left columns). The 3D morphology we observed using $HRAS^{V12}$ MCF10A cells resembles that reported for mouse mammary cells expressing oncogenic RAS and grown in a 3D collagen matrix (16).

To inhibit autophagy in this experimental system, we stably expressed unique short-hairpin RNAs (shRNA) against two autophagy genes (ATGs)—*ATG7* (shATG7-1 and shATG7-2) or *ATG12* (shATG12) in MCF10A cells expressing $HRAS^{V12}$. ATG7 or ATG12 knockdown decreased target protein levels, reduced basal and starvation (HBSS) induced autophagy, and increased protein levels of the autophagy substrate p62/SQSTM1 (Fig S1B-E). In 3D culture, the invasive protrusions observed with oncogenic RAS activation were profoundly attenuated in ATG deficient cells. Instead, $HRAS^{V12}$ shATG structures were spherical in morphology, similar to non-transformed BABE controls (Fig. 1A-B). Decreased invasive protrusions following autophagy inhibition were also observed upon stable *ATG3* knockdown (shATG3), and upon treatment with chloroquine or bafilomycin A, two lysosomal inhibitors that block the late steps of autophagy (Fig. S1F). Importantly, ATG knockdown in $HRAS^{V12}$ cells did not affect RAS expression or activation associated phosphorylation of the major downstream effector MAPK/ERK (Fig. S1G). Thus, the reduction in 3D invasive protrusions following ATG knockdown is not due to decreased expression or activity of oncogenic RAS.

The disruption of basement membrane integrity is a hallmark of carcinoma invasion *in vivo* (14). To corroborate whether the protrusions we observed in $HRAS^{V12}$-transformed 3D cultures represented invasive behavior, we first evaluated basement membrane integrity by examining the expression and localization of the basement membrane protein LAMA5 (laminin 5) in $HRAS^{V12}$-derived acini. Consistent with previous reports, control non-transformed MCF10A acini (BABE) displayed polarized deposition of LAMA5 onto the basal surface (Fig. 2A, left panels) (15). In contrast, the expression of $HRAS^{V12}$ resulted in cytosolic accumulation of LAMA5, with no evidence of polarized deposition at the cell-ECM interface. Notably, this aberrant cytosolic staining pattern was especially prominent in the protrusions of $HRAS^{V12}$ cultures. Correlating with the decreased formation of invasive protrusions, ATG knockdown restored polarized LAMA5 secretion; based on this marker, most individual structures in ATG deficient $HRAS^{V12}$ cultures were encompassed by an intact basement membrane (Fig. 2A). Hence, in addition to restricting the formation of invasive protrusions, autophagy inhibition restored polarized basement membrane secretion typically absent in $HRAS^{V12}$ shCNT structures.

To extend these results, we evaluated ECM proteolytic activity in control and autophagy-deficient $HRAS^{V12}$ cultures by assessing fluorescence emanating from the proteolytic cleavage of dye-quenched collagen IV (COL4). In control non-transformed acini (BABE), we observed a faint ring of fluorescence surrounding each structure, corresponding to COL4 degradation due to the normal outgrowth of acini during 3D morphogenesis. On the other hand, $HRAS^{V12}$ shCNT-expressing structures exhibited high levels of fluorescence that extended well beyond the immediate vicinity of individual structures (Fig. 2B). Notably, streaks of fluorescence connecting adjacent structures were frequently observed in $HRAS^{V12}$ shCNT cultures (Fig. 2B), which resembled the networks of invasive protrusions (Fig 1B). In contrast, $HRAS^{V12}$ shATG-derived structures exhibited a ring-like COL4 degradation pattern that was restricted to the cell-ECM interface, similar to that observed in non-transformed controls (Fig. 2B). Thus, the absence of morphological protrusions in ATG deficient $HRAS^{V12}$ cultures was associated with the restoration of basement membrane integrity and reduced ECM proteolytic activity. Together, these findings corroborate that autophagy supports RAS-driven invasion in 3D culture.

ATG depletion in $HRAS^{V12}$ structures does not promote apoptosis or proliferation arrest in 3D culture

We next evaluated the impact of autophagy inhibition on oncogenic RAS-driven proliferation and cell survival. During normal MCF10A acinar morphogenesis, autophagy

inhibition results in the enhanced apoptosis of cells occupying the luminal space (17). To test whether autophagy deficiency similarly impacted apoptosis in $HRAS^{V12}$ structures, we immunostained structures with an antibody against cleaved CASP3 (caspase-3). In contrast to the robust luminal apoptosis observed in control acini (BABE), only isolated cleaved CASP3 positive cells were observed in $HRAS^{V12}$ shCNT structures, consistent with the ability of oncogenic RAS to promote cell survival in 3D culture (Fig 3A). Upon enumerating cleaved CASP3 positive cells from these 3D cultures, we found that ATG knockdown did not significantly impact apoptosis in comparison to shCNT cultures (Fig. 3A). To assess whether autophagy inhibition potentially impacted non-apoptotic death processes, we also stained day 8 3D cultures with ethidium bromide (EtBr), an intravital dye that is incorporated into all dying cells. Whereas acini derived from non-transformed (BABE) cells displayed high levels of EtBr staining corresponding to luminal cell death (Fig. 3B), $HRAS^{V12}$ structures displayed only occasional EtBr cells scattered throughout the structures. Although ATG knockdown in $HRAS^{V12}$ cultures resulted in spherical structures that lacked invasive protrusions, we did not observe any increase in EtBr staining in these cultures (Fig. 3B). Thus, in contrast to normal and oncogenic PIK3CA MCF10A acinar morphogenesis, autophagy inhibition does not promote apoptosis in RAS-transformed 3D structures (17, 18).

To evaluate the effects of autophagy inhibition on the proliferative capacity of $HRAS^{V12}$ structures, we immunostained cultures with the proliferation marker Ki67 on day 8, a timepoint at which normal MCF10A acini exhibit reduced proliferation (19). As expected, low levels of Ki67 positive cells were observed in BABE structures (Fig 3C, left panels). However, both control and autophagy deficient $HRAS^{V12}$ structures displayed high levels of Ki67 positive cells (Fig 3C). Overall, these results indicate that although autophagy deficiency potently restricts $HRAS^{V12}$ driven invasion, it does not universally suppress the diverse oncogenic effects of $HRAS^{V12}$ in 3D culture, including the ability of activated RAS to inhibit apoptosis and sustain proliferation.

Autophagy supports oncogenic RAS-driven cell migration in vitro and pulmonary metastasis in vivo

Because defects in invasive capacity are often associated with diminished cell motility, we next measured cell migration in autophagy competent and deficient epithelial cells. Upon ATG depletion, $HRAS^{V12}$ MCF10A cells demonstrated an approximately 30% reduction in migratory capacity in a monolayer wound-healing assay of cell migration (Fig. 4A). Similar results were obtained using a transwell migration assay, which demonstrated a significant decrease in migration of ATG knockdown cells (Fig. 4B). We further corroborated these results using MDA-MB-231 cells, a highly migratory, KRAS mutant breast cancer cell line. siRNA-mediated knockdown of either ATG7 or ATG12 in MDA-MB-231 cells resulted in reduced LC3-II formation (Fig. S1H) as well as decreased wound closure (Fig. 4C, left). A similar decrease in MDA-MB-231 migration was also observed in the presence of the lysosomal inhibitor bafilomycin A (Fig. 4C, right). Therefore, in addition to supporting invasion of $HRAS^{V12}$ MCF10A cells in 3D culture, autophagy facilitates the migration of cells expressing oncogenic RAS in monolayer culture. Finally, we utilized an experimental metastasis assay to evaluate whether the effects of autophagy inhibition on invasion and migration correlated with changes in metastatic capacity in vivo; in support, the ability of $HRAS^{V12}$ MCF10A cells to produce pulmonary metastases was reduced upon ATG knockdown (Fig 4D).

Altered differentiation of $HRAS^{V12}$ MCF10A cells upon autophagy inhibition

Constitutive RAS activation alters epithelial differentiation by driving an epithelial-mesenchymal transition (EMT) (20, 21), a process associated with increased invasive and

migratory capacity *in vitro* and with metastatic capacity *in vivo* (13). Therefore, we evaluated how autophagy inhibition affects protein expression changes associated with RAS-induced EMT. We isolated BABE, $HRAS^{V12}$ shCNT and $HRAS^{V12}$ shATG expressing cells from day 8 3D cultures and determined the protein expression of a panel of EMT associated genes by immunobloting. In comparison to nontransformed BABE acini, $HRAS^{V12}$ shCNT structures displayed decreased KRT14 (keratin 14), an epithelial marker, and a corresponding increase in the mesenchymal protein VIM (vimentin) (Fig S2A). ATG knockdown reversed these $HRAS^{V12}$-driven changes in differentiation, resulting in an increase in KRT14 protein levels and a corresponding decrease in VIM levels compared to $HRAS^{V12}$ shCNT cells isolated from 3D culture (Fig. S2A). However, autophagy inhibition had minimal effects on other EMT markers that were altered by oncogenic RAS expression. Only a slight increase in CDH1 (E-cadherin) was observed in shATG cells, decreased FN1 (fibronectin) was only observed in shATG7-1 expressing cells, and CDH2 (N-cadherin) levels were unchanged following ATG knockdown (Fig. S2A).

During EMT, cells commonly lose the ability to form cell-cell junctions (22). Therefore, we analyzed the effects of autophagy inhibition on cell-cell junctional integrity in $HRAS^{V12}$ 3D structures by immunostaining for CTNNB1 (β-catenin). Normal MCF10A acini (BABE) displayed strong β-catenin staining at cell-cell contacts, indicating intact adherens junctions, whereas the expression of $HRAS^{V12}$ resulted in a near-complete loss of β-catenin junctional staining; in these cultures, only isolated focal areas of junctional β-catenin staining were observed (Fig. S2B). Upon ATG knockdown in $HRAS^{V12}$ structures, both the expression and junctional localization of β-catenin were significantly restored (Fig. S2B). Based on these results, we conclude that autophagy inhibition modulates certain aspects of mesenchymal differentiation in RAS-transformed cells in 3D culture, most notably the suppression of VIM, as well as the restoration of KRT14 expression and epithelial cell-cell contacts. Nonetheless, autophagy deficiency does not broadly suppress RAS-driven EMT.

ATG knockdown in $HRAS^{V12}$ cells inhibits the production of pro-invasive secreted factors in 3D culture

Cell migration and invasion involves the secretion of multiple factors that cooperate to promote motility and to degrade the surrounding ECM (23, 24). To ascertain if defects in RAS-driven invasion observed following autophagy suppression were the result of decreased production of pro-invasive factors, we performed a co-culture assay in which $HRAS^{V12}$ shATG7-1 cells (co-expressing GFP for tracking purposes) were combined with $HRAS^{V12}$ shCNT cells at a ratio of 3:1, respectively. Whereas $HRAS^{V12}$ shATG7-1-GFP cells cultured alone grew as spherical structures (Fig. 5A, left panels), upon co-culture with $HRAS^{V12}$ shCNT cells, $HRAS^{V12}$ shATG7-1-GFP structures became dispersed and formed invasive protrusions (Fig. 5A, right panels). Hence, we hypothesized that factors from neighboring $HRAS^{V12}$ shCNT cells are sufficient to rescue *in trans* the invasion defect in $HRAS^{V12}$ shATG7-1 cells. To further test this prediction, we grew $HRAS^{V12}$ shATG cells in 3D culture for 3 days and subsequently treated these structures with conditioned media (CM) produced from either BABE or $HRAS^{V12}$ shCNT cultures. $HRAS^{V12}$ shATG structures remained as compact spheres following treatment with BABE CM (Fig. 5B, Fig. S3A). In contrast, CM from $HRAS^{V12}$ shCNT cultures elicited invasive protrusions at 24h following treatment, which became fully evident by 72h (Fig. 5B, Fig. S3A); notably, CM addition did not induce invasion in non-transformed BABE acini (Fig. S3B). Furthermore, basement membrane integrity was lost in $HRAS^{V12}$ shATG cells treated with $HRAS^{V12}$ CM (Fig. 5C). These findings demonstrate that autophagy inhibition in $HRAS^{V12}$ cells inhibits the production of secreted factors required for RAS-driven invasion in 3D culture.

Diminished secretion of IL6 contributes to reduced invasion in autophagy deficient HRAS^{V12} cells

During RAS-induced senescence, ATG depletion inhibits IL6 production following acute oncogenic RAS activation in IMR90 fibroblasts, indicating autophagy supports the production of IL6 in response to oncogenic RAS activation (25). Because IL6 has been demonstrated to support RAS-driven tumorigenesis, promote migration and invasion, and also drive epithelial-mesenchymal transition (26-28), we tested whether IL6 levels were altered in HRAS^{V12} shATG 3D cultures. Analysis of IL6 in conditioned media collected from 3D cultures by ELISA indicated a significant reduction in secreted IL6 levels in HRAS^{V12} shATG-expressing cultures compared to HRAS^{V12} shCNT cultures (Fig. 6A). Furthermore, this decrease in secreted IL6 was not the result of reduced *IL6* gene expression; in fact, qPCR analysis revealed that *IL6* transcript levels in HRAS^{V12} shATG cells were increased, rather than decreased, in comparison to HRAS^{V12} shCNT cells (Fig 6B). Notably, studies of RAS-induced senescence similarly demonstrated that autophagy deficient cells exhibit reduced IL6 protein levels due to impaired translation, rather than transcription (25, 29). In contrast, we uncovered that ATG depletion did not attenuate IL6 protein levels in RAS-transformed cells grown in 3D culture (Fig 6C). These results suggest that autophagy facilitates IL6 secretion during HRAS^{V12} 3D morphogenesis.

To ascertain the functional significance of these results, we interrogated whether IL6 was necessary for HRAS^{V12}-driven invasion in 3D culture. First, we treated HRAS^{V12} shATG structures with HRAS^{V12} shCNT CM in the presence versus absence of an IL6 function-blocking antibody. The addition of IL6 function-blocking antibody attenuated the ability of HRAS^{V12} shCNT CM to promote invasive protrusions in HRAS^{V12} shATG cultures, whereas an IgG isotype control had no effect (Fig. 6D). In parallel, we tested how exogenous recombinant human IL6 (rhIL6) treatment affected HRAS^{V12} shATG cells during 3D morphogenesis. rhIL6 addition did not affect nontransformed BABE acini (Fig. S3C) but partly restored invasion in HRAS^{V12} shATG cultures, resulting in large globular structures, increased invasive protrusions, and loss of basement membrane integrity (Fig. 6E, S3D-E). Also, rhIL6 addition partially reversed the effects of autophagy inhibition on KRT14 and VIM expression in HRAS^{V12} shATG7 cells (Fig. S3F). Hence, our results suggest that autophagy promotes efficient IL6 secretion by HRAS^{V12} cells in 3D culture, which is necessary for invasion.

Autophagy facilitates *MMP2* and *WNT5A* expression by HRAS^{V12} cells in 3D culture

In addition to identifying a defect in IL6 production following ATG knockdown, we performed a qPCR array to measure the expression levels of genes involved in EMT and invasion, and identified *WNT5A* and *MMP2* as two candidate factors whose expression was upregulated in HRAS^{V12} cells relative to BABE cells but potently suppressed upon autophagy inhibition. qPCR analysis of cells collected from 3D cultures confirmed a 2-fold decrease in *MMP2* and *WNT5A* expression in HRAS^{V12} shATG cells compared to HRAS^{V12} shCNT (Fig. 7A and B). Notably, we also evaluated the effects of rhIL6 treatment on *MMP2* and *WNT5A* expression in shATG7-1 cultures and found this was not sufficient to rescue expression, indicating that regulation of these factors was independent of IL6 (Fig. S3G).

Because these secreted factors have been implicated in cell migration and invasion, we further evaluated whether their decreased expression following ATG knockdown also contributed to the reduced invasive potential of HRAS^{V12} shATG cells. First, we utilized gelatin zymography to assess MMP2 activity in CM from 3D cultures. MMP2 activity was enhanced in HRAS^{V12} cells compared to non-transformed (BABE) controls, and upon ATG knockdown in HRAS^{V12} cells, this activity was reduced (Fig. 7C). The increase in MMP2

expression and secretion following constitutive RAS activation was necessary for RAS-driven invasion, as addition of an MMP2 inhibitor, Arp-100, was sufficient to inhibit the formation of invasive protrusions in $HRAS^{V12}$ 3D cultures (Fig. 7D). Furthermore, the decrease in *WNT5A* expression correlated with a decrease in WNT5A protein levels in $HRAS^{V12}$ shATG cells isolated from 3D culture (Fig. 7E). Moreover, the addition of recombinant WNT5A to $HRAS^{V12}$ shATG7-1 3D cultures promoted the dissociation of cells within the structures and enhanced the formation of invasive protrusions (Fig. 7F). Thus, in addition to IL6, autophagy facilitates the production of multiple secreted pro-migratory and invasive factors that support RAS-driven invasion in 3D culture.

DISCUSSION

Our results delineate a previously unrecognized function for autophagy in facilitating oncogenic RAS-driven invasion and migration. Using a 3D culture system, we demonstrate that suppression of autophagy in $HRAS^{V12}$ MCF10A cells restricts the formation of invasive protrusions, restores basement membrane integrity, and attenuates ECM proteolysis. In addition, autophagy inhibition diminishes cell migration *in vitro* and pulmonary metastasis *in vivo*. Upon treatment with conditioned media produced from autophagy-competent $HRAS^{V12}$ cells, invasion is completely restored in autophagy-deficient $HRAS^{V12}$ cultures, indicating that autophagy mediates the production of secreted factors that drive invasion in oncogenic cells. In further support, we uncover that autophagy inhibition elicits the coordinate reduction of multiple molecules favoring invasion. Overall, these findings expand our understanding of how autophagy supports cancer progression.

Although autophagy inhibition suppresses invasion in 3D culture, it does not ubiquitously revert oncogenic RAS-driven changes in cell behavior. Indeed, MAPK activation remains unaltered following autophagy inhibition in this 3D culture model and moreover, the oncogenic activation of RAS continues to disrupt fundamental aspects of 3D morphogenesis in autophagy deficient cells. First, autophagy inhibition does not alter the ability of $HRAS^{V12}$ to suppress apoptosis in 3D culture. Moreover, autophagy inhibition does not suppress proliferation in $HRAS^{V12}$ 3D cultures; rather, the spherical structures from $HRAS^{V12}$ ATG knockdown cells remain highly proliferative over extended periods. Remarkably, both others and we have shown that ATG depletion reduces soft agar growth and attenuates the proliferation of RAS-transformed cells grown in monolayer (3-5, 30); hence, the absence of proliferative suppression in this 3D culture model may be context dependent. These results also differ from those obtained in KRAS mutant mouse cancer models in which genetic ATG deletion impairs proliferation and, in certain cases, enhances apoptosis (4, 6, 7). Certain reasons may explain these differences. First, we have only reduced ATGs using RNAi, rather than genetically eliminated these proteins. Second, the experiments here are significantly shorter duration in comparison to autophagy deficient K-Ras tumor growth *in vivo.*

Although previous studies have demonstrated that autophagy supports the invasion of glioblastoma cells, the mechanistic underpinnings remain unclear (31, 32). Cell invasion requires the production and secretion of factors that stimulate migration and degrade the surrounding ECM (24). Upon treatment of autophagy depleted $HRAS^{V12}$ cells with conditioned media produced from their autophagy competent counterparts, the ability to form invasive protrusions is completely restored, suggesting that autophagy is required for the efficient production of secreted factors that promote invasion and migration of $HRAS^{V12}$ cells. Notably, conditioned media treatment does not promote invasion in nontransformed BABE cells, indicating oncogenic Ras pathway activation is still required for invasion.

Importantly, we identify IL6 as one critical factor whose secretion is ATG dependent; our results substantiate that this pro-invasive cytokine is necessary to restore invasion in autophagy-deficient $HRAS^{V12}$ cells. They also point to a specific role for autophagy in facilitating IL6 secretion; upon ATG knockdown, RAS-transformed cells fail to secrete IL6 into the conditioned media, yet both IL6 transcription and translation remain intact. These results differ from recent studies of oncogenic RAS-mediated senescence, in which reduced IL6 secretion in autophagy-deficient cells is proposed to be secondary to decreased protein synthesis (25, 29).

Though traditionally viewed as an autodigestive process, growing evidence suggests new roles for autophagy in both conventional and unconventional secretion (33). Indeed, a genetic role for ATGs has been implicated in: 1) unconventional secretion of proteins lacking N-terminal ER signal sequences (34-37); 2) efficient egress of secretory lysosomes (38, 39); and 3) conventional secretion of growth factors (40, 41). Further dissecting how autophagy directs the secretion of IL6 and other factors during RAS transformation remains an important topic for future study. Remarkably, IL6 re-addition only partially restores invasion and mesenchymal differentiation in $HRAS^{V12}$ autophagy-deficient cultures, indicating other factors promote invasion. In support, these cells exhibit reduced levels of other pro-invasive molecules, including WNT5A and MMP2. In contrast to reduced IL6 secretion, which is likely a proximal event following ATG knockdown, these changes in WNT5A and MMP2 result from decreased gene expression, indicating that autophagy inhibition produces broader transcriptional changes contributing to reduced invasion by $HRAS^{V12}$ cells.

Recently, the deletion of *RB1CC1/FIP200*, a gene mediating autophagosome initiation, was demonstrated to reduce lung metastases in the MMTV-PyMT breast cancer model. However, since *RB1CC1* deletion profoundly restricted primary tumor growth, it was unclear whether decreased metastasis was secondary to reduced primary tumor burden (12). In addition, although liver-specific deletion of *ATG7* or *ATG5* initiates the development of benign adenomas, these tumors are unable to progress to adenocarcinomas, suggesting that autophagy is required for advanced tumor progression (42, 43). Here, in epithelial cells transformed with oncogenic RAS, we demonstrate that defective autophagy results in decreased invasion and migration, which correlates with the reduced ability to metastasize *in vivo.* Although our results do not rule out potentially important functions for autophagy in disseminated cell survival or outgrowth at foreign tissue sites, they delineate new roles for autophagy in the control of secretion during carcinoma progression.

EXPERIMENTAL PROCEDURES

Cell lines

MCF10A cells were obtained from the American Tissue Culture Collection (ATCC) and cultured as previously described (44). MDA-MB-231 cells were obtained from the ATCC and cultured in DMEM supplemented with 10% FBS, penicillin, and streptomycin. Cell lines were passaged for less than 6 months following resuscitation and were not authenticated.

Three dimensional culture assays

MCF10A overlay 3D culture was performed as previously described (44). As indicated, the following reagents were added to cultures: 500ng/mL WNT5A (R&D Systems), 200ng/mL IL6 (Peprotech), 25 μg/mL anti-IL6 function blocking antibody (R&D Systems), 25 μg/mL IgG control antibody (BD Biosciences), 25μM Arp-100 (Santa Cruz Biotechnology), 5μM chloroquine diphosphate salt (Sigma), and 5nM bafilomycin A (Sigma). For the 3D ECM

degradation assay, human DQ-COL4 (Invitrogen) was mixed with Matrigel to a final concentration of 25μg/mL prior to plating. To collect cells for immunoblotting and RNA isolation, cultures were incubated with 0.25% Trypsin/EDTA at 37°C for 10 min to dissociate cells from surrounding matrix and create a single cell suspension. Cells were resuspended in media containing 20% serum and washed twice with PBS to remove residual Matrigel.

For co-culture assays, shATG7-1 was expressed in $HRAS^{V12}$ cells stably expressing pBABEhygro GFP. This GFP-labeled "target" cell line was then cultured in isolation or combined with unlabelled (pBABEhygro) $HRAS^{V12}$ shCNT cells at a ratio of 3:1 with total cell number kept constant at 7,500 cells/well. For conditioned media (CM) experiments, $HRAS^{V12}$ shATG expressing cells were grown in 3D culture for 3d; subsequently, the media was replaced with conditioned media harvested from BABE or $HRAS^{V12}$ shCNT MCF10A cells grown in 3D culture for 6-8 days. When indicated, 25 μg/mL anti-IL6 function blocking or IgG isotype control antibody was added to the CM.

Wounding Assay

Cells were grown to confluence in 3.5 cm dishes and incubated overnight in assay media lacking EGF for MCF10A cells or DMEM+2% FBS for MDA-MB-231 cells. Wound healing was performed in the presence of 2μg/ml mitomycin C (Sigma). Cells were wounded with a 200μl pipette tip and imaged at time of wounding (0 h) and the indicated time points. Average wound widths were measured at each time point and decreases in wound width were calculated by subtracting the average width at the final time point from the average width at 0 h using MetaMorph Software (v6.0).

Transwell Assay

Cells were starved overnight in assay media lacking EGF and then plated at 1.0×10^5 in the top chamber of an 8μm Transwell filter in assay media lacking EGF. The bottom chamber was filled with assay medium containing 5 ng/ml EGF. Cells were allowed to migrate for 24 h, after which the top of each filter was cleared of cells. Cells attached to the bottom of the filter were fixed and stained with crystal violet. Crystal violet was extracted with 10% acetic acid and the absorbance was measured at 600 nm.

Experimental metastasis assay

For experimental metastasis assays, cells were infected with pHIV-ZsGreen (Addgene, Cambridge, MA, plasmid 18121). 1.0×10^6 $HRAS^{V12}$ shCNT, shATG7-1, and shATG12 cells stably expressing ZsGreen were injected into the tail vein of NOD/SCID mice. After 140 days, whole lungs were fixed and imaged to detect the number of ZsGreen positive foci per lung. All animal experiments were conducted in accordance with approved UCSF IACUC protocols.

IL6 ELISA

Day 5 3D cultures were washed twice with PBS and cultured for 18 h in serum-free media. Conditioned media was collected, and total protein levels were determined by BCA assay (Thermo Scientific) to normalize samples. IL6 levels were measured using the Quantikine High Sensitivity ELISA kit (R&D Systems).

Statistical analyses

Each experiment was repeated at least three independent times. GraphPad Prism software (v5.0b) was used for generation of graphs and statistical analysis. *P* values were determined by Student's t-test or ANOVA as stated.

Supplementary Material

Refer to Web version on PubMed Central for supplementary material.

Acknowledgments

Grant support to JD includes the NIH (R01CA126792 and −S1), the DOD BCRP (W81XWH-11-1-0130 and W81XWH-12-1-0505), Samuel Waxman Cancer Research Foundation, and the California TRDRP (18XT-0106). RL was supported by a DOD BCRP Predoctoral Award (W81XWH-08-1-0759) and CMK by a Genentech Fellowship, University of California CRCC Fellowship, and NIH F31CA167905.

Abbreviations

(ECM)	Extracellular matrix
(ATG)	autophagy-related gene
(EMT)	epithelial-mesenchymal transition

REFERENCES

1. Schubbert S, Shannon K, Bollag G. Hyperactive Ras in developmental disorders and cancer. Nat Rev Cancer. 2007; 7:295–308. [PubMed: 17384584]
2. Pylayeva-Gupta Y, Grabocka E, Bar-Sagi D. RAS oncogenes: weaving a tumorigenic web. Nat Rev Cancer. 2011; 11:761–74. [PubMed: 21993244]
3. Lock R, Roy S, Kenific CM, Su JS, Salas E, Ronen SM, et al. Autophagy facilitates glycolysis during Ras-mediated oncogenic transformation. Mol Biol Cell. 2011; 22:165–78. [PubMed: 21119005]
4. Yang S, Wang X, Contino G, Liesa M, Sahin E, Ying H, et al. Pancreatic cancers require autophagy for tumor growth. Genes Dev. 2011; 25:717–29. [PubMed: 21406549]
5. Guo JY, Chen HY, Mathew R, Fan J, Strohecker AM, Karsli-Uzunbas G, et al. Activated Ras requires autophagy to maintain oxidative metabolism and tumorigenesis. Genes Dev. 2011; 25:460–70. [PubMed: 21317241]
6. Guo JY, Karsli-Uzunbas G, Mathew R, Aisner SC, Kamphorst JJ, Strohecker AM, et al. Autophagy suppresses progression of K-ras-induced lung tumors to oncocytomas and maintains lipid homeostasis. Genes Dev. 2013; 27:1447–61. [PubMed: 23824538]
7. Rosenfeldt MT, O'Prey J, Morton JP, Nixon C, MacKay G, Mrowinska A, et al. p53 status determines the role of autophagy in pancreatic tumour development. Nature. 2013; 504:296–300. [PubMed: 24305049]
8. Kimmelman AC. The dynamic nature of autophagy in cancer. Genes Dev. 2011; 25:1999–2010. [PubMed: 21979913]
9. Chen N, Debnath J. Autophagy and tumorigenesis. FEBS Lett. 2010; 584:1427–35. [PubMed: 20035753]
10. Degenhardt K, Mathew R, Beaudoin B, Bray K, Anderson D, Chen G, et al. Autophagy promotes tumor cell survival and restricts necrosis, inflammation, and tumorigenesis. Cancer cell. 2006; 10:51–64. [PubMed: 16843265]
11. Amaravadi RK, Lippincott-Schwartz J, Yin XM, Weiss WA, Takebe N, Timmer W, et al. Principles and current strategies for targeting autophagy for cancer treatment. Clin Cancer Res. 2011; 17:654–66. [PubMed: 21325294]
12. Wei H, Wei S, Gan B, Peng X, Zou W, Guan JL. Suppression of autophagy by FIP200 deletion inhibits mammary tumorigenesis. Genes Dev. 2011; 25:1510–27. [PubMed: 21764854]
13. Polyak K, Weinberg RA. Transitions between epithelial and mesenchymal states: acquisition of malignant and stem cell traits. Nat Rev Cancer. 2009; 9:265–73. [PubMed: 19262571]
14. Debnath J, Brugge JS. Modelling glandular epithelial cancers in three-dimensional cultures. Nat Rev Cancer. 2005; 5:675–88. [PubMed: 16148884]

15. Debnath J, Mills KR, Collins NL, Reginato MJ, Muthuswamy SK, Brugge JS. The role of apoptosis in creating and maintaining luminal space within normal and oncogene-expressing mammary acini. Cell. 2002; 111:29–40. [PubMed: 12372298]
16. Oft M, Peli J, Rudaz C, Schwarz H, Beug H, Reichmann E. TGF-beta1 and Ha-Ras collaborate in modulating the phenotypic plasticity and invasiveness of epithelial tumor cells. Genes & development. 1996; 10:2462–77. [PubMed: 8843198]
17. Fung C, Lock R, Gao S, Salas E, Debnath J. Induction of Autophagy during Extracellular Matrix Detachment Promotes Cell Survival. Mol Biol Cell. 2008; 19:797–806. [PubMed: 18094039]
18. Chen N, Eritja N, Lock R, Debnath J. Autophagy restricts proliferation driven by oncogenic phosphatidylinositol 3-kinase in three-dimensional culture. Oncogene. 2012
19. Muthuswamy SK, Li D, Lelievre S, Bissell MJ, Brugge JS. ErbB2, but not ErbB1, reinitiates proliferation and induces luminal repopulation in epithelial acini. Nature cell biology. 2001; 3:785–92.
20. Thiery JP. Epithelial-mesenchymal transitions in development and pathologies. Current opinion in cell biology. 2003; 15:740–6. [PubMed: 14644200]
21. Shin S, Dimitri CA, Yoon SO, Dowdle W, Blenis J. ERK2 but not ERK1 induces epithelial-to-mesenchymal transformation via DEF motif-dependent signaling events. Molecular cell. 2010; 38:114–27. [PubMed: 20385094]
22. Xu J, Lamouille S, Derynck R. TGF-beta-induced epithelial to mesenchymal transition. Cell Res. 2009; 19:156–72. [PubMed: 19153598]
23. Scheel C, Eaton EN, Li SH, Chaffer CL, Reinhardt F, Kah KJ, et al. Paracrine and autocrine signals induce and maintain mesenchymal and stem cell States in the breast. Cell. 2011; 145:926–40. [PubMed: 21663795]
24. Friedl P, Wolf K. Tumour-cell invasion and migration: diversity and escape mechanisms. Nat Rev Cancer. 2003; 3:362–74. [PubMed: 12724734]
25. Young AR, Narita M, Ferreira M, Kirschner K, Sadaie M, Darot JF, et al. Autophagy mediates the mitotic senescence transition. Genes Dev. 2009; 23:798–803. [PubMed: 19279323]
26. Ancrile B, Lim KH, Counter CM. Oncogenic Ras-induced secretion of IL6 is required for tumorigenesis. Genes & development. 2007; 21:1714–9. [PubMed: 17639077]
27. Leslie K, Gao SP, Berishaj M, Podsypanina K, Ho H, Ivashkiv L, et al. Differential interleukin-6/Stat3 signaling as a function of cellular context mediates Ras-induced transformation. Breast Cancer Res. 2010; 12:R80. [PubMed: 20929542]
28. Sullivan NJ, Sasser AK, Axel AE, Vesuna F, Raman V, Ramirez N, et al. Interleukin-6 induces an epithelial-mesenchymal transition phenotype in human breast cancer cells. Oncogene. 2009; 28:2940–7. [PubMed: 19581928]
29. Narita M, Young AR, Arakawa S, Samarajiwa SA, Nakashima T, Yoshida S, et al. Spatial coupling of mTOR and autophagy augments secretory phenotypes. Science (New York, NY.). 2011; 332:966–70.
30. Kim MJ, Woo SJ, Yoon CH, Lee JS, An S, Choi YH, et al. Involvement of autophagy in oncogenic K-Ras-induced malignant cell transformation. J Biol Chem. 2011; 286:12924–32. [PubMed: 21300795]
31. Galavotti S, Bartesaghi S, Faccenda D, Shaked-Rabi M, Sanzone S, McEvoy A, et al. The autophagy-associated factors DRAM1 and p62 regulate cell migration and invasion in glioblastoma stem cells. Oncogene. 2013; 32:699–712. [PubMed: 22525272]
32. Macintosh RL, Timpson P, Thorburn J, Anderson KI, Thorburn A, Ryan KM. Inhibition of autophagy impairs tumor cell invasion in an organotypic model. Cell Cycle. 2012; 11:2022–9. [PubMed: 22580450]
33. Deretic V, Jiang S, Dupont N. Autophagy intersections with conventional and unconventional secretion in tissue development, remodeling and inflammation. Trends Cell Biol. 2012; 22:397–406. [PubMed: 22677446]
34. Duran JM, Anjard C, Stefan C, Loomis WF, Malhotra V. Unconventional secretion of Acb1 is mediated by autophagosomes. The Journal of cell biology. 2010; 188:527–36. [PubMed: 20156967]

35. Manjithaya R, Anjard C, Loomis WF, Subramani S. Unconventional secretion of Pichia pastoris Acb1 is dependent on GRASP protein, peroxisomal functions, and autophagosome formation. The Journal of cell biology. 2010; 188:537–46. [PubMed: 20156962]

36. Manjithaya R, Subramani S. Autophagy: a broad role in unconventional protein secretion? Trends Cell Biol. 2011; 21:67–73. [PubMed: 20961762]

37. Dupont N, Jiang S, Pilli M, Ornatowski W, Bhattacharya D, Deretic V. Autophagy-based unconventional secretory pathway for extracellular delivery of IL-1beta. EMBO J. 2011; 30:4701–11. [PubMed: 22068051]

38. Ushio H, Ueno T, Kojima Y, Komatsu M, Tanaka S, Yamamoto A, et al. Crucial role for autophagy in degranulation of mast cells. J Allergy Clin Immunol. 2011; 127:1267–76 e6. [PubMed: 21333342]

39. DeSelm CJ, Miller BC, Zou W, Beatty WL, van Meel E, Takahata Y, et al. Autophagy proteins regulate the secretory component of osteoclastic bone resorption. Dev Cell. 2011; 21:966–74. [PubMed: 22055344]

40. Ebato C, Uchida T, Arakawa M, Komatsu M, Ueno T, Komiya K, et al. Autophagy is important in islet homeostasis and compensatory increase of beta cell mass in response to high-fat diet. Cell Metab. 2008; 8:325–32. [PubMed: 18840363]

41. Jung HS, Chung KW, Won Kim J, Kim J, Komatsu M, Tanaka K, et al. Loss of autophagy diminishes pancreatic beta cell mass and function with resultant hyperglycemia. Cell Metab. 2008; 8:318–24. [PubMed: 18840362]

42. Takamura A, Komatsu M, Hara T, Sakamoto A, Kishi C, Waguri S, et al. Autophagy-deficient mice develop multiple liver tumors. Genes Dev. 2011; 25:795–800. [PubMed: 21498569]

43. Inami Y, Waguri S, Sakamoto A, Kouno T, Nakada K, Hino O, et al. Persistent activation of Nrf2 through p62 in hepatocellular carcinoma cells. J Cell Biol. 2011; 193:275–84. [PubMed: 21482715]

44. Debnath J, Muthuswamy SK, Brugge JS. Morphogenesis and oncogenesis of MCF-10A mammary epithelial acini grown in three-dimensional basement membrane cultures. Methods (San Diego, Calif.). 2003; 30:256–68.

SIGNIFICANCE

Our results delineate a previously unrecognized function for autophagy in facilitating oncogenic RAS-driven invasion. We demonstrate that an intact autophagy pathway is required for the elaboration of multiple secreted factors favoring invasion, including IL6.

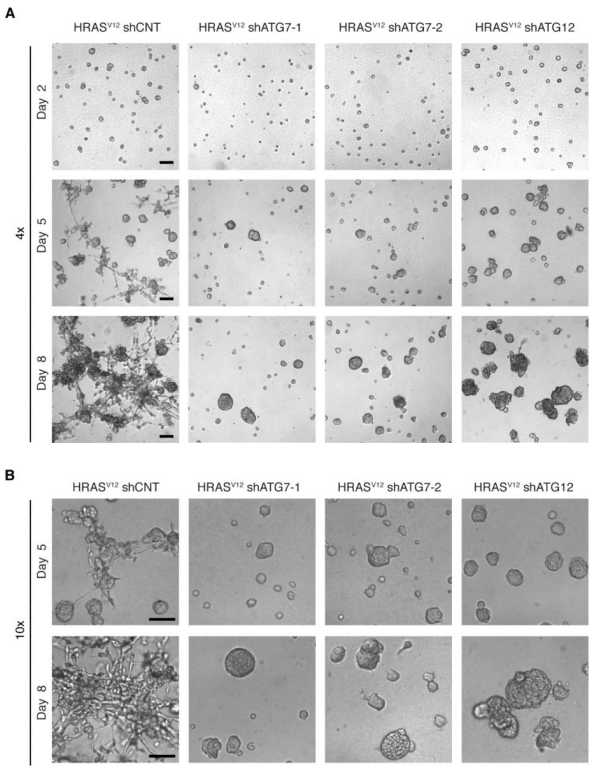

Figure 1. Autophagy is required for the formation of invasive protrusions mediated by HRAS^{V12} in 3D culture

(A-B) HRAS^{V12} MCF10A cells stably expressing non-targeting control shRNA (shCNT) or shRNAs against autophagy genes (shATGs) were 3D cultured on Matrigel for the indicated number of days. Representative phase contrast images at the indicated magnifications are shown. Bar, 100μm.

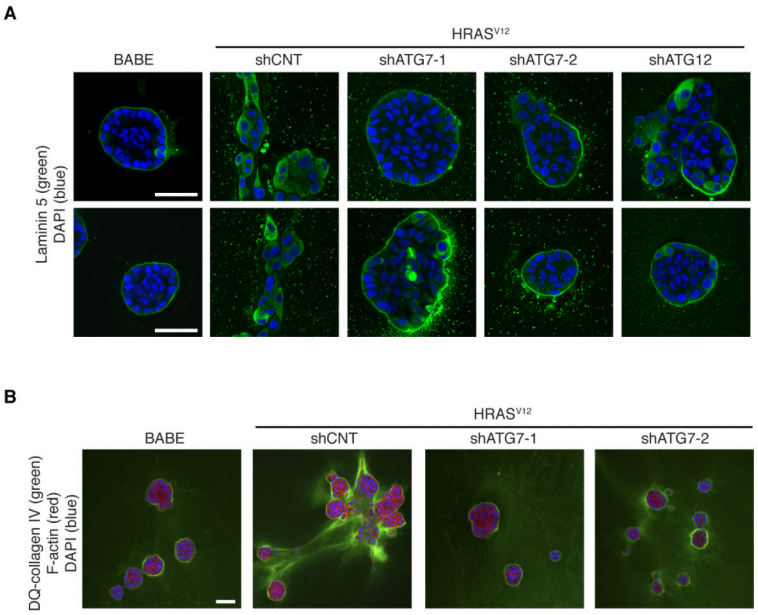

Figure 2. Autophagy inhibition in HRAS^{V12} cells restores basement membrane integrity and restricts ECM proteolysis in 3D culture

(A) HRAS^{V12} cells expressing shCNT or shATGs were 3D cultured on Matrigel for 8 days. Structures were fixed and immunostained with antibodies against the basement membrane protein LAMA5 (human specific), counterstained with DAPI to detect nuclei, and imaged by confocal microscopy. Two representative images of each condition are shown. Bar, 50μm. (B) HRAS^{V12} MCF10A cells were 3D cultured on Matrigel containing 25μg/mL fluorescein DQ-collagen IV (DQ-COL4) for 5 days. Structures were fixed, counterstained with phalloidin (to visualize F-actin) and DAPI, and imaged by confocal microscopy. Green fluorescence represents areas of proteolytic cleavage of the DQ-COL4 present in the ECM. Bar, 50μm.

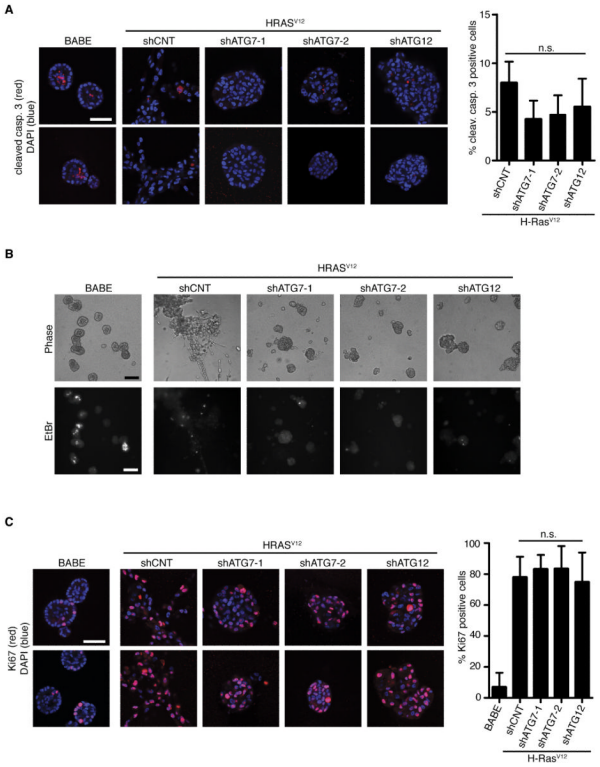

Figure 3. Autophagy inhibition in HRAS^{V12} MCF10A structures does not promote apoptosis or proliferation arrest

(A) Left: Two representative images of day 8 3D cultures of BABE and HRAS^{V12} MCF10A cells expressing shCNT or shATGs immunostained with antibody against cleaved CASP3 and counterstained with DAPI to detect nuclei. Bar, 50μm. Right: Quantification of cleaved CASP3 positive cells present within 3D cultures of each indicated cell type (mean +/− s.d., Student's t-test). (B) Representative phase (top) and corresponding wide-field fluorescence (bottom) images of BABE and HRAS^{V12} cells expressing shCNT or shATGs stained with the intravital dye ethidium bromide (EtBr). Bar, 100μm. (C) Left: Two representative images of day 8 3D cultures of BABE and HRAS^{V12} cells expressing shCNT or shATGs immunostained with antibody against Ki67 and DAPI counterstained. Bar, 50μm. Right: Quantification of Ki67 positive nuclei present within 3D cultures of each indicated cell type (mean +/− s.d., Student's t-test).

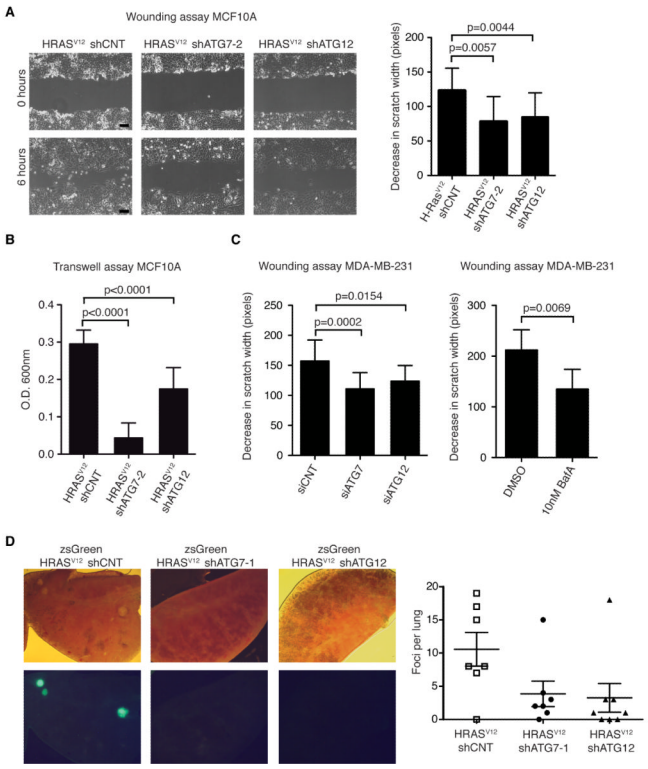

Figure 4. ATG knockdown suppresses the motility and reduces the metastatic potential of cells expressing oncogenic RAS

(A) Representative images (left) and quantification (right) of wounding assay on HRAS^{V12} MCF10A cells expressing shCNT or shATGs. Confluent monolayers were scratched and wound width was measured at 0 and 6h after initial wounding to quantify the decrease in scratch width. (mean +/− s.d., Student's t-test, shCNT n=16, shATG7-2 n=8, shATG12 n=14). Bar, 100μm. (B) Transwell migration of HRAS^{V12} MCF10A cells expressing shCNT or shATGs. 24h after plating, cells that migrated to the bottom of the filter were stained with crystal violet. Results are expressed as the mean crystal violet extracted from stained cells (mean +/− s.d., Student's t-test, n=9). (C) Wounding assays of MDA-MB-231 cells expressing siATGs or in presence of 10nM bafilomycin A (BafA). Graphs represent the decrease in scratch width at 10h and 9h after initial wounding, respectively (mean +/− s.d., Student's t-test, siCNT n=16, siATG7 n=16, siATG12 n=10, DMSO n=6, BafA n=6). (D) Representative images (left) and quantification (right) of ZsGreen positive metastatic foci following tail vein injection of ZsGreen expressing HRAS^{V12} shCNT, shATG7-1 or shATG12 cells (mean +/− s.e.m., shCNT n=7, shATG7-1 n=7, shATG12 n=8).

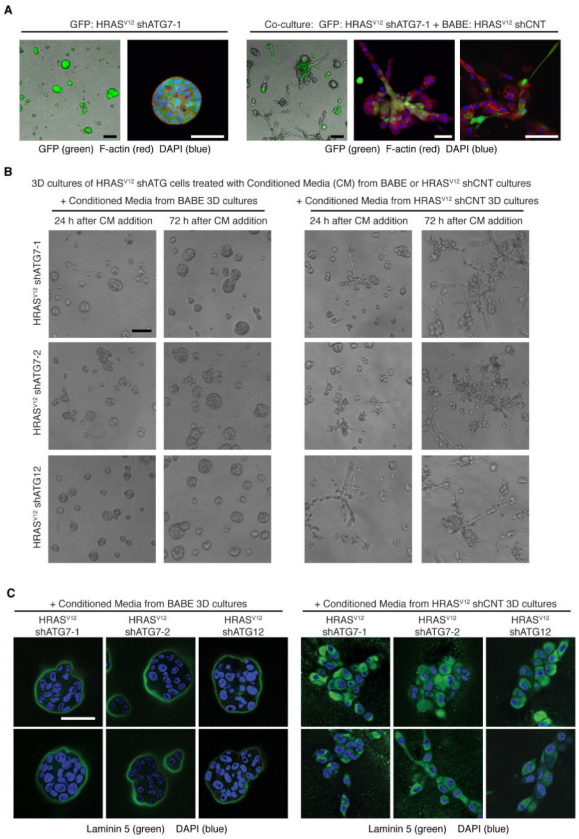

Figure 5. ATG knockdown in HRAS^{V12} cells inhibits the production of pro-invasive secreted factors in 3D culture

(A) 3D co-culture of HRAS^{V12} shATG7-1 with HRAS^{V12} shCNT cells rescues invasion of HRAS^{V12} shATG7-1 cells. HRAS^{V12} shATG7-1 cells expressing GFP were cultured for 8 days in 3D either alone (left) or together with HRAS^{V12} shCNT cells expressing an empty vector (BABE). Structures were imaged by phase contrast and wide-field fluorescence microscopy or fixed, counterstained with phalloidin (to visualize F-actin) and DAPI and imaged by confocal microscopy. Phase: Bar, 100μm. Confocal: Bar, 50 μm. (B) HRAS^{V12} MCF10A cells expressing shATGs were cultured in 3D for 3d and subsequently treated with BABE or HRAS^{V12} shCNT conditioned media (CM). Representative phase contrast images at 24h and 72h following the addition of CM. Bar, 100μm. (C) 3D cultures of HRAS^{V12} MCF10A cells expressing shATGs were treated with BABE or HRAS^{V12} shCNT CM for 72h; thereafter, cultures were fixed and immunostained with an antibody against LAMA5 (human specific) to detect basement membrane and DAPI counterstained. Two representative images per condition are shown. Bar, 50μm.

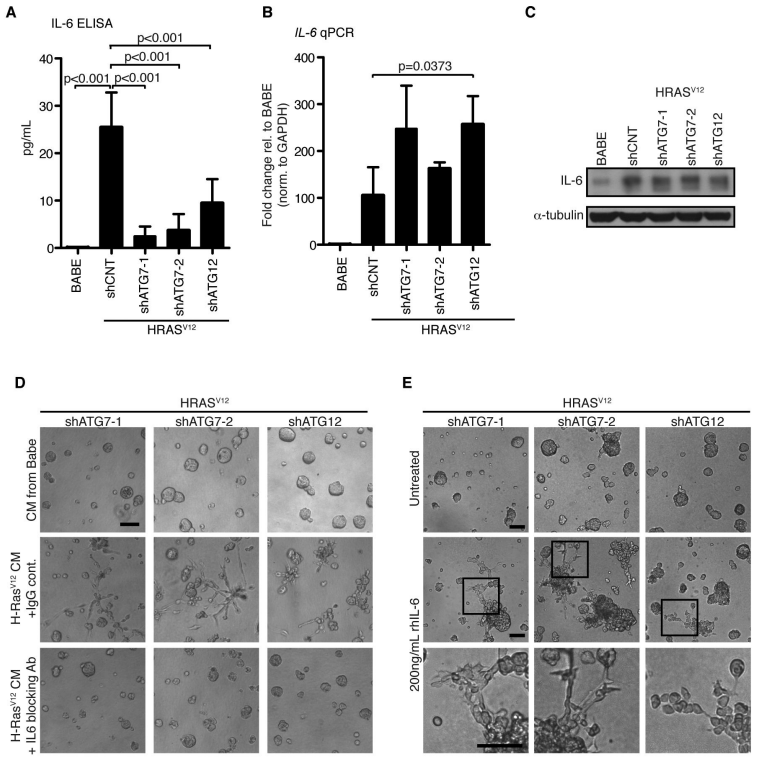

Figure 6. Autophagy supports IL6 secretion necessary for oncogenic RAS-driven invasion in 3D culture

(A) Levels of IL6 in conditioned media collected on day 6 from 3D cultures of the indicated cell types. (mean +/− s.d., ANOVA, BABE n=3, $HRAS^{V12}$ n=5). (B) *IL6* expression levels normalized to *GAPDH* in cells collected from day 8 3D cultures. (mean relative to BABE +/− s.d., Student's t-test, n=3). (C) IL6 protein levels in day 8 3D cultures from the indicated cell types. (D) Representative phase contrast images of $HRAS^{V12}$ shATG 3D cultures treated for 48h with BABE CM (top) or with $HRAS^{V12}$ shCNT CM containing an IL6 function-blocking antibody (bottom) or IgG control antibody (middle). Bar, 100μm. (E) Representative phase contrast images of $HRAS^{V12}$ shATG 3D cultures grown in the presence or absence of 200ng/mL recombinant human IL6 for 7d. Bar, 100μm.

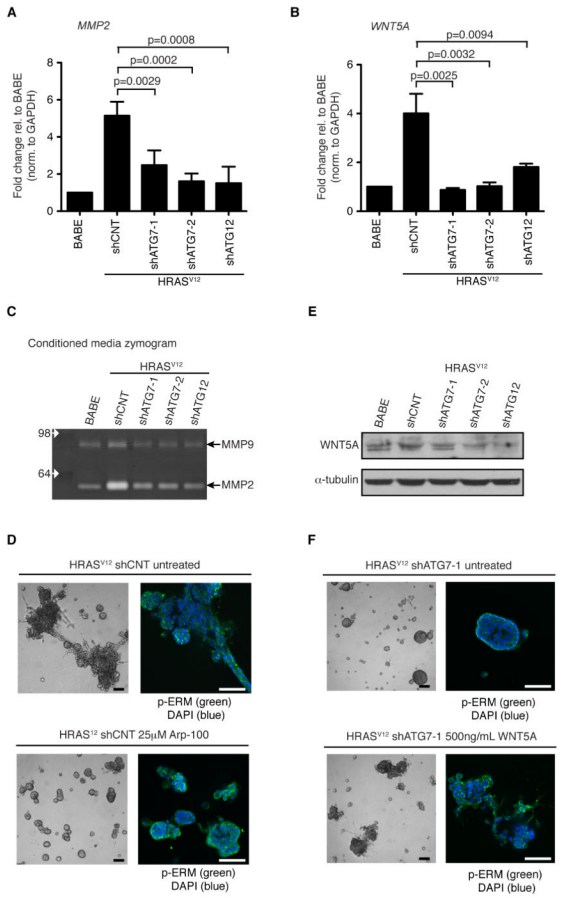

Figure 7. WNT5A and MMP2 are reduced following autophagy inhibition in 3D culture

(A-B) RNA was isolated from BABE, HRAS^{V12} shCNT, and HRAS^{V12} shATG cells cultured in 3D for 8 days. Expression levels of *MMP2* and *WNT5A* were determined by qPCR and normalized to an internal control *GAPDH*. Results represent the mean relative to BABE +/− s.d. (*MMP2*, n=4; *WNT5A*, n=3; Student's t-test). (C) Conditioned media was collected from BABE, HRAS^{V12} shCNT and HRAS^{V12} shATG cells grown in 3D culture. Activity levels of MMP9 and MMP2 in the conditioned media were determined by zymography. (D) HRAS^{V12} shCNT cells were grown in the absence (top) or presence (bottom) of 25μm Arp-100. Left: Structures were imaged on day 8 by phase contrast microscopy. Right: Representative confocal images of structures immunostained with anti-phospho-ERM (P-ERM) to detect cell borders and counterstained with DAPI. Bars, 100μm. (E) BABE, HRAS^{V12} shCNT, and HRASV12 shATG cells were collected from 3D culture on day 8, lysed, and protein levels of WNT5A were determined by immunoblot analysis. (F) HRAS^{V12} shATG7-1 cells were grown in 3D for 8 days in the absence (top) or presence (bottom) of 500ng/mL WNT5A. Left: Representative phase contrast images. Right: Representative confocal images of structures immunostained with anti-phospho-ERM to detect cell borders and counterstained with DAPI. Bars, 100μm.